Bulletin of Mathematical Biology (2022) 84:21
https://doi.org/10.1007/s11538-021-00974-5

Society for Mathematical Biology

ORIGINAL ARTICLE

Extinction of Bistable Populations is Affected by the Shape of their Initial Spatial Distribution

Yifei Li[1] · Stuart T. Johnston[2] · Pascal R. Buenzli[1] · Peter van Heijster[3] · Matthew J. Simpson[1]

Received: 18 January 2021 / Accepted: 15 November 2021 / Published online: 20 December 2021

Abstract

The question of whether biological populations survive or are eventually driven to extinction has long been examined using mathematical models. In this work, we study population survival or extinction using a stochastic, discrete lattice-based random walk model where individuals undergo movement, birth and death events. The discrete model is defined on a two-dimensional hexagonal lattice with periodic boundary conditions. A key feature of the discrete model is that crowding effects are introduced by specifying two different crowding functions that govern how local agent density influences movement events and birth/death events. The continuum limit description of the discrete model is a nonlinear reaction-diffusion equation, and we focus on crowding functions that lead to linear diffusion and a bistable source term that is often associated with the strong Allee effect. Using both the discrete and continuum modelling tools, we explore the complicated relationship between the long-term survival or extinction of the population and the initial spatial arrangement of the population. In particular, we study different spatial arrangements of initial distributions: (i) a well-mixed initial distribution where the initial density is independent of position in the domain; (ii) a vertical strip initial distribution where the initial density is independent of vertical position in the domain; and, (iii) several forms of two-dimensional initial distributions where the initial population is distributed in regions with different shapes. Our results indicate that the shape of the initial spatial distribution of the population affects extinction of bistable populations. All software required to solve the discrete and continuum models used in this work are available on GitHub.

✉ Matthew J. Simpson
matthew.simpson@qut.edu.au

1 School of Mathematical Sciences, Queensland University of Technology, Brisbane, Australia

2 Systems Biology Laboratory, School of Mathematics and Statistics, and Department of Biomedical Engineering, Melbourne School of Engineering, University of Melbourne, Parkville, Victoria, Australia

3 Biometris, Wageningen University and Research, Wageningen, The Netherlands

Keywords Population dynamics · Birth · Death · Movement · Reaction-diffusion · Survival

1 Introduction

The classical logistic growth model is widely adopted in mathematical biology and mathematical ecology (Kot 2001; Murray 2002; Edelstein-Keshet 2005). In the logistic model, small initial population densities increase over time to approach a maximum carrying-capacity density (Maini et al. 2004a, b). An implicit assumption in using the logistic growth model is that any population, no matter how small, will always grow and survive. This limitation also applies to models based on the weak Allee effect, which incorporates a reduced per-capita growth rate relative to the logistic model when the density is small (Taylor and Hastings 2005). To address this limitation, more complicated models have been developed, including models based on the strong Allee effect (Allee and Bowen 1932; Lewis and Kareiva 1993; Stephens et al. 1999; Courchamp et al. 1999; Taylor and Hastings 2005; Courchamp et al. 2008; Arroyo-Esquivel and Hastings 2020). In the strong Allee effect model, initial densities greater than a threshold, called the *Allee threshold*, grow to eventually reach the carrying capacity, whereas initial densities less than the Allee threshold eventually go extinct (Allee and Bowen 1932; Courchamp et al. 1999; Taylor and Hastings 2005; Courchamp et al. 2008; Fadai and Simpson 2020). This kind of population dynamics, also referred to as *bistable* population dynamics (Kot 2001), is often adopted to model situations where the potential for population extinction is thought to be important (Saltz and Rubenstein 1995; Courchamp et al. 1999; Drake 2004; Böttger et al. 2015; Vortkamp et al. 2020). Bistable population dynamics are often studied using mathematical models that take the form of an ordinary differential equation (ODE). In this case, the eventual extinction or survival of the population is dictated solely by whether the initial density is greater than, or less than, the Allee threshold density. Such ODE models assume that the population is well-mixed, and hence neglect spatial effects. Spatial effects, such as moving invasion fronts, can be incorporated by considering partial differential equation (PDE) models where the density of individuals depends explicitly upon position and time (Lewis and Kareiva 1993; Holmes et al. 1994; Hastings et al. 2005). A common PDE framework is to consider a reaction-diffusion equation (RDE) with a cubic bistable source term (Neufeld et al. 2017; Johnston et al. 2017).

When spatial effects are taken into consideration, even the logistic model with linear diffusion may not always lead to the survival of populations. For example, for a population on a finite domain with homogeneous Dirichlet boundary conditions, the population will go extinct when reproduction cannot balance the loss through boundaries (Skellam 1951; Grindrod 1996). The size of the domain must exceed a critical value, called the *critical patch size*, so that a population persists (Holmes et al. 1994; Lutscher 2019). Similar results also hold for diffusing bistable populations, where loss through the boundaries is not the only mechanism of interest since the source term can become negative (Bradford and Philip 1970a, b). For a population governed by the strong Allee effect, enough individuals must aggregate together so that the population can reproduce and balance the loss due to the death of individuals.

This motivates the concept of the *critical initial area* (also known as critical aggregation or critical initial radius) which indicates that the initial population can only survive if the initial occupied area and the initial density are sufficiently large (Lewis and Kareiva 1993; Soboleva et al. 2003; Lewis et al. 2016). See Table 1 for a brief review of relevant models and known results.

Current RDE models of bistable populations on two-dimensional domains often consider an infinite domain and a radially symmetric initial distribution (Lewis and Kareiva 1993; Petrovskii and Shigesada 2001). In particular, Lewis and Kareiva (1993) use formal asymptotics to derive expressions for the critical initial area for a radially distributed bistable population with linear diffusion, and their results are valid in the limit that the time scale of reproduction is much faster than the time scale of migration. In contrast, here we develop a mathematical modelling framework for studying bistable population dynamics on two-dimensional domains with periodic boundary conditions. Using this framework, we extend the previous results by showing that bistable populations with the same initial area can either lead to survival or extinction depending upon the initial shape of the population distribution.

Our modelling framework is based on a two-dimensional stochastic discrete random walk model on a hexagonal lattice (Jin et al. 2016; Fadai et al. 2020). The discrete model is an exclusion process, so that each lattice site can be occupied by no more than one agent. Individuals in the model undergo a birth-death process that is modulated by localised crowding effects (Jin et al. 2016; Johnston et al. 2017). The continuum limit of the discrete model leads to a two-dimensional RDE with a bistable source term. This framework allows us to explore discrete simulations together with solutions of the RDE. This approach is convenient because the discrete model is more realistic in the sense that it incorporates fluctuations, but this benefit incurs additional computational overhead (West et al. 2016; Macfarlane et al. 2018; Chaplain et al. 2020). Moreover, the discrete framework provides additional information such as the age structure and individual trajectories which cannot be easily obtained using a continuum approach. In contrast, the continuum RDE model can be solved numerically very efficiently, but the continuum approach is only accurate if the time scale of migration is small compared to the time scale of proliferation (Simpson et al. 2010). Moreover, the continuum RDE model does not provide any information about the role of stochasticity (West et al. 2016; Macfarlane et al. 2018; Chaplain et al. 2020). So, to take advantages of both approaches, we use both a stochastic model and the continuum limit description.

In all cases, we study population dynamics on a square domain of side length L, with periodic boundary conditions along all boundaries. We explore the role of the initial population distribution by considering different initial spatial arrangements of agents. We first distribute agents uniformly across the entire domain as shown in Fig. 1a, which leads to a well-mixed population. For the vertical strip initial distribution, we distribute agents uniformly within a column of width w_1 as shown in Fig. 1b, which may represent a population of individuals along a one-dimensional river environment (Lutscher et al. 2010). For the initial distributions restricted in both spatial dimensions, we first consider a simple shape and distribute agents uniformly within a square region of area $w_1 \times w_1$ as shown in Fig. 1c, which may represent a population of cells in a scratch assay (Treloar et al. 2014). We further consider several other initial spatial arrangements of agents, see Figs. 6–8.

Table 1 The comparison of models studying the critical initial area or critical patch size (Bradford and Philip 1970a, b) and our model. All models include the strong Allee effect, while Etienne et al. (2002) further consider a competition mechanism

References	Model	Coordinate	Domain	Boundary conditions	Initial conditions	Properties
Bradford and Philip (1970a)	$\frac{\partial C(x,t)}{\partial t} = \frac{\partial^2 C(x,t)}{\partial x^2} + f(C(x,t))$,	One-dimensional Cartesian	$0 \le x < L$ where $L < \infty$ or $L \to \infty$	Homogeneous Neumann at $x = 0$	No initial conditions for the steady-state solution $C(x)$.	There exist stable steady-state solutions, which represent population survival, if L and $C(0)$ are greater than the thresholds.
	where f is a general bistable form.			Homogeneous or inhomogeneous Dirichlet at $x = L$	Perturbed steady-state solutions for stability analysis.	
Bradford and Philip (1970b)	$\frac{\partial C(r,t)}{\partial t} = \frac{1}{r}\frac{\partial}{\partial r}\left(r\frac{\partial C(r,t)}{\partial r}\right) + f(C(r,t))$,	Two-dimensional, radially symmetric	$0 \le r < R$ where $R < \infty$ or $R \to \infty$	Homogeneous Neumann at $r = 0$	No initial conditions for the steady-state solution $C(r)$.	There exist stable steady-state solutions, which represent population survival, if L and $C(0)$ are greater than the thresholds.
	where f is a general bistable form.			Homogeneous or inhomogeneous Dirichlet at $r = R$	Perturbed steady-state solutions for stability analysis.	The threshold of $C(0)$ is significantly greater than it in Bradford and Philip (1970a).

Table 1 continued

References	Model	Coordinate	Domain	Boundary conditions	Initial conditions	Properties
Lewis and Kareiva (1993)	$\frac{\partial C(x,y,t)}{\partial t} = D\nabla^2 C(x,y,t) + kC(1-C)(C-A)$	Two-dimensional Cartesian	$\mathbb{R}^2$	Homogeneous Neumann	$C = 1$ in a square region and $C = 0$ elsewhere.	Numerical simulations indicate that the initial distribution converges to a travelling wave solution.
				Homogeneous Dirichlet	$C = 1$ in a circular region with radius r^*, and $C = 0$ elsewhere.	There exists a threshold $r_{\min}$ determined by D, k and A. If $r^* > r_{\min}$, the initial distribution forms a radially expanding wave which leads to population survival; if $r^* < r_{\min}$, the initial distribution forms a radially shrinking wave which leads to population extinction.
Soboleva et al. (2003)	$\frac{\partial C(x,y,t)}{\partial t} = D\nabla^2 C(x,y,t) + f(C(x,y,t)),$	Two-dimensional Cartesian	$\mathbb{R}^2$	Homogeneous Dirichlet	Perturbed radially symmetric unstable steady-state solutions.	The unstable steady-state solution provides a threshold initial distribution where populations above the threshold distribution will survive and populations below the threshold distribution will go extinct.
	where f is cubic and bistable with $f(0) = f(1) = 0$.			Perturbed radially asymmetric unstable steady-state solutions.		The symmetric one-dimensional threshold distribution has a smaller maximum density relative to the radially symmetric two-dimensional threshold distribution.

Table 1 continued

References	Model	Coordinate	Domain	Boundary conditions	Initial conditions	Properties
Kot et al. (1996)	Integrodifference eq. (discrete time n, continuous space x): $C^{n+1}(x) = \int_{-\infty}^{\infty} k(x - \hat{x}) f[C^n(\hat{x})]\mathrm{d}\hat{x}$, where $f = 0$ if $0 < C^n < C_\mathrm{A}$ and $f = K$ if $C_\mathrm{A} < C^n < K$.	One-dimensional Cartesian	$-\infty < x < \infty$	Homogeneous Dirichlet	$C = B$ for $-l^* < x < l^*$ and $C = 0$ elsewhere.	The initial distribution will form an expanding travelling wave front, which leads to population survival, if $B > C_\mathrm{A}$ and if l^* is greater than a threshold.
Etienne et al. (2002)	Integrodifference eq. (discrete time n, continuous space x, y):	Two-dimensional Cartesian	$[0, L] \times [0, L]$	Periodic	$C = B$ in the whole domain.	Numerical simulations indicate that the initial distribution and density of individuals, resource availability and heterogeneity influence the fate of populations.
	$L^{n+1}(x, y) = g(R) \iint_{\Omega} k(x - \hat{x}, y - \hat{y}) A^n(\hat{x}, \hat{y})\mathrm{d}\hat{x}\mathrm{d}\hat{y}$,			Homogeneous Neumann	$C = B$ in different-sized central square regions and $C = 0$ elsewhere.	
	where $A^n = 0$ if $L^n < L_\mathrm{min}$ or $L^n > L_\mathrm{max}$ and $A^n = L^n/2$ elsewhere. Here, L^n is the larval population in generation n, A^n is the female adult population in generation n and $g(R)$ represents the resource availability.			Homogeneous Dirichlet		

Table 1 continued

References	Model	Coordinate	Domain	Boundary conditions	Initial conditions	Properties
Li et al. (2021) (this paper)	Discrete model with the continuum limit	Two-dimensional Cartesian	$[0, L] \times [0, L]$	Periodic	$C = B$ in the whole domain.	Both discrete and numerical simulations indicate that initial shapes affect the fate of populations. The key feature of these shapes is their dimensionality.
	$\frac{\partial C(x, y, t)}{\partial t} = D\nabla^2 C(x, y, t) + kC(1 - C)(C - A)$				$C = B$ in regions with different shapes and $C = 0$ elsewhere.	

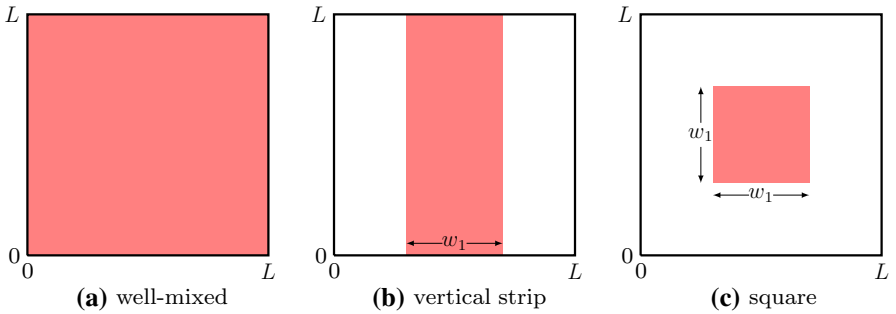

Fig. 1 Initial spatial distributions of the population with different shapes on an $L \times L$ square domain. In (**a**), individuals are distributed uniformly across the entire $L \times L$ domain. In (**b**), individuals are distributed uniformly in a vertical strip of width w_1 and height L. In (**c**), individuals are distributed uniformly in the central square region of length and width w_1

This work is organised as follows. In Sect. 2, we describe the discrete individual-based model, paying particular attention to incorporating realistic movement and growth mechanisms. For simplicity, we use the generic term *growth* to refer to the birth/death process in the discrete model. The reason why we make a distinction between birth and death will become clear when we describe the modelling framework. In Sect. 3, we explain how to analyse the discrete model using a mean-field assumption to arrive at an approximate continuum limit description in terms of a classical RDE. Our discrete-continuous framework incorporates crowding functions into both movement and birth/death mechanisms, which extends the previous work that only considers a crowding function in birth/death mechanisms (Jin et al. 2016). Moreover, our model is very flexible since it describes a wide range of movement and birth/death mechanisms influenced by crowding effects. Results in Sect. 4 show how both the discrete and continuum models compare. In Sect. 5, we systematically explore how population survival or extinction depends upon the shape of the initial distribution. All software required to solve the discrete and continuum models used in this work are available on GitHub.

2 Discrete Model

We consider a lattice-based discrete model describing movement, birth and death events in a population of individuals on a hexagonal lattice, with lattice spacing $\Delta > 0$. Each lattice site is indexed by (i, j) and has a unique Cartesian coordinate,

$$(x, y) = \begin{cases} \left(i\Delta, j\dfrac{\Delta\sqrt{3}}{2} \right), & \text{if } j \text{ is even,} \\ \left(\left(i + \dfrac{1}{2} \right) \Delta, j\dfrac{\Delta\sqrt{3}}{2} \right), & \text{if } j \text{ is odd.} \end{cases} \tag{1}$$

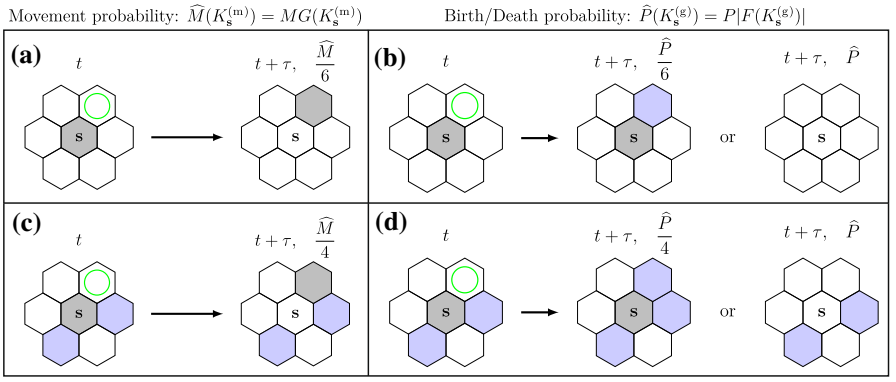

Fig. 2 Movement and birth/death mechanisms. In each lattice fragment site **s** is occupied and shaded in grey, and occupied neighbouring sites are shaded in blue, while vacant neighbouring sites are unshaded (white). In (**a**), the agent at site **s** moves with probability $\widehat{M}$ and moves to the target site, highlighted with a green circle, with probability $\widehat{M}/6$. In (**b**), the agent at site **s** undergoes a birth event with probability $\widehat{P}$ and places a new agent on the target site with probability $\widehat{P}/6$ if the growth crowding function $F > 0$. In contrast, it dies with probability $\widehat{P}$ if $F < 0$. In (c), the agent moves with probability $\widehat{M}$ and moves to the target site with probability $\widehat{M}/4$. In (d), the agent undergoes a birth event with probability $\widehat{P}$ and places a new agent on the target site with probability $\widehat{P}/4$ if $F > 0$. In contrast, it dies with probability $\widehat{P}$ if $F < 0$ (Color figure online)

In any single realisation of the stochastic model, a lattice site **s** is either occupied, $C_{\mathbf{s}} = 1$, or vacant, $C_{\mathbf{s}} = 0$. If there are $Q(t)$ agents on the lattice at time t, we advance the stochastic simulation from time t to time $t + \tau$ by randomly selecting $Q(t)$ agents, one at a time, with replacement, so that any particular agent may be selected more than once, and allowing those agents to *attempt* to move. Once the $Q(t)$ potential movement events have been assessed, we then select $Q(t)$ agents at random, one at a time, with replacement, to *attempt* to undergo a growth event, which could be either a birth or death event depending upon the local crowding conditions. Although altering the order of these events leads to different outcomes in particular discrete simulations, these differences are not important when we consider averaged data from many identically prepared realisations of the model (Simpson et al. 2009a, b).

We now explain some features of the discrete model in terms of the schematic in Fig. 2. In this initial description of the discrete model, we consider nearest-neighbour movement and growth events only, and we will relax this assumption later. Fig. 2a shows a potential movement event for an agent at site **s**, where all nearest-neighbour sites are vacant. In this case, the probability of attempting to move during the next time step of duration τ is $M \in [0, 1]$, and the attempted motility event will be successful with probability $\hat{M} \leq M$. Here, we note that the two probabilities, M and $\hat{M}$ are, in general, different. This difference is a result of the local crowding effects. The special case in Fig. 2a where the agent at site **s** is uncrowded we have $\hat{M} = M$. If the attempted motility event is successful, the agent at site s moves to a randomly chosen vacant site chosen among the set of vacant nearest-neighbour sites. In this case, as all six neighbour sites are vacant, the probability of moving to the target site, highlighted with a green circle, is $\hat{M}/6$.

In Fig. 2b, we show a potential growth event for an agent at site $\mathbf{s}$, where again all nearest-neighbour sites are vacant. Here, the probability of attempting to grow in the next time step of duration τ is $P \in [0, 1]$, and the attempted growth event is successful with probability $\hat{P} \leq P$. Again, the difference between P and $\hat{P}$ is caused by local crowding effects, and since this agent is uncrowded, we have $\hat{P} = P$. If the attempted growth event is successful, there are two possible outcomes. First, the growth event is a birth event. In this case, a daughter agent is placed at a randomly chosen vacant site within the set of nearest-neighbour sites with probability $\hat{P}$. As there are six vacant neighbour sites, the probability of placing a daughter agent at the target site, highlighted in green, is $\hat{P}/6$. Second, the growth event is a death event, and the agent is removed from the lattice, with probability $\hat{P}$. The distinction between the birth and death events is governed by the sign of the *growth crowding function*, F, which will be explained later.

To illustrate how crowding effects are incorporated into the movement component of the model, we now consider the schematic in Fig. 2c, where the agent at site $\mathbf{s}$ is surrounded by two agents, highlighted in purple. The probability of attempting to move is $M \in [0, 1]$, and the attempted movement event is successful with probability $\hat{M} = MG(K_{\mathbf{s}}^{(\mathrm{m})})$. Here, $K_{\mathbf{s}}^{(\mathrm{m})}$ is a measure of the local density of site $\mathbf{s}$, and $G(K_{\mathbf{s}}^{(\mathrm{m})}) \in [0, 1]$ is the *movement crowding function* that specifies how the local density influences the probability of this agent to undergo a movement event. If this attempt is successful, as there are four vacant neighbour sites, the probability of moving to the target site, highlighted in green, is $\hat{M}/4$.

Figure 2d illustrates how crowding effects are incorporated into the growth component of the model, where the agent at site $\mathbf{s}$ is surrounded by two agents. The probability of attempting to grow is $P \in [0, 1]$, and the attempted growth is successful with probability $\hat{P} = P|F(K_{\mathbf{s}}^{(\mathrm{g})})|$. Here, $K_{\mathbf{s}}^{(\mathrm{g})}$ is again a measure of the local density of site $\mathbf{s}$ and the function $F(K_{\mathbf{s}}^{(\mathrm{g})}) \in [-1, 1]$ is called the growth crowding function that specifies how the local density influences the probability of this agent to undergo a growth event. If this attempt is successful, there are two possible outcomes reflected by the sign of F. If $F > 0$, the growth event is a birth event, and a daughter agent is placed at a randomly chosen vacant site with probability $\hat{P}$. As there are four vacant neighbour sites, the probability of placing a daughter agent at the vacant target site, highlighted in green, is $\hat{P}/4$. Second, if $F < 0$, the growth event is a death event, and the agent is removed from the lattice with probability $\hat{P}$. The special case where $F = 0$ leads to neither a birth or death event.

A key feature of our model is in the way that the local density about each site affects movement and growth events through the movement and growth crowding functions. To describe this, we take $\mathcal{N}_r\{\mathbf{s}\}$ to denote the set of neighbouring sites around site $\mathbf{s}$, where $r \geq 1$ is the integer number of concentric rings of sites surrounding site $\mathbf{s}$, so that $|\mathcal{N}_r| = 3r(r + 1)$ (Jin et al. 2016; Fadai et al. 2020). The probability that any potential movement or growth event is successful depends upon the crowdedness of the local region surrounding site $\mathbf{s}$. We count neighbouring agents in $\mathcal{N}_r$ and consider

$$K_{\mathbf{s}}(r) = \frac{1}{|\mathcal{N}_r|} \sum_{\mathbf{s}' \in \mathcal{N}_r\{\mathbf{s}\}} C_{\mathbf{s}'} \in [0, 1], \tag{2}$$

as a simple measure of the crowdedness of the local region surrounding site $\mathbf{s}$. While in Fig. 2, we explain the model with $r = 1$ and $|\mathcal{N}_1| = 6$, it is possible to use different-sized templates, depending on the choice of r. Sometimes it is useful to use different-sized templates for the movement and growth mechanisms. For example, Simpson et al. (2010) argues that cell movement can be modelled using a nearest-neighbour random walk with $r = 1$, whereas cell proliferation often involves non-nearest-neighbour interactions since daughter cells are often deposited several cell diameters away from the location of the mother cell. This argument is supported by experimental images of cell proliferation where careful examination of timelapse movies shows that daughter cells are often generated some distance from the mother cell (Druckenbrod and Epstein 2005). To simulate such dynamics, Simpson et al. (2010) introduce proliferation mechanisms where daughter agents are placed up to four lattice sites away from the mother agent to faithfully capture this biological detail into their model. This would be similar to setting $r = 1$ for movement and $r = 4$ for growth in our model. It is thus convenient for us to make a notational distinction between the size of the templates for motility and growth. Therefore, we denote the motility template as $K_{\mathbf{s}}^{(\mathrm{m})} = K_{\mathbf{s}}(r')$ and the growth template as $K_{\mathbf{s}}^{(\mathrm{g})} = K_{\mathbf{s}}(r'')$ where $r' \geq 1$ and $r'' \geq 1$ are two, potentially different, positive integers.

We now describe the details of how crowding effects and different-sized spatial templates are incorporated into the growth component of the model with reference to the schematic illustration in Fig. 3. Note that this figure only indicates the potential growth events without the indication of any movement events. In Fig. 3a–c, crowding of the agent at site $\mathbf{s}$ is measured using a nearest-neighbour template with $r = 1$ and the growth crowding function $F(K_{\mathbf{s}}^{(\mathrm{g})}) = 1 - K_{\mathbf{s}}^{(\mathrm{g})}$, as given in Fig. 3d. The probability of undergoing a birth event is $\hat{P} = P|F(K_{\mathbf{s}}^{(\mathrm{g})})|$. In Fig. 3a where $K_{\mathbf{s}}^{(\mathrm{g})} = 0$, we have $F(0) = 1$ and $\hat{P} = P$. As there are six vacant sites in $\mathcal{N}_1$, the probability of placing a daughter agent at the target site, highlighted in green, is $\hat{P}/6$. In Fig. 3b, where the agent at site $\mathbf{s}$ is surrounded by two neighbour agents, the probability of undergoing a birth event is $\hat{P} = 2P/3$, since $K_{\mathbf{s}}^{(\mathrm{g})} = 1/3$ and $F(1/3) = 2/3$. As there are four vacant sites in $\mathcal{N}_1$, the probability of placing a daughter agent at the target site is $\hat{P}/4$. Similarly, in Fig. 3c, we have $\hat{P} = P/3$ as $K_{\mathbf{s}}^{(\mathrm{g})} = 2/3$ and $F(2/3) = 1/3$. As there are two vacant sites in $\mathcal{N}_1$, the probability of placing a daughter agent at the target site is $\hat{P}/2$.

In Figures 3e–g, we introduce a non-nearest-neighbour growth mechanism by measuring the crowdedness of the agent at site $\mathbf{s}$ using a larger spatial template with $r = 2$. Therefore, if the agent at $\mathbf{s}$ undergoes a successful birth event, the daughter agent is able to be placed at any vacant site within $\mathcal{N}_2$. The probability of undergoing a birth event is $\hat{P} = P|F(K_{\mathbf{s}}^{(\mathrm{g})})|$, where $F(K_{\mathbf{s}}^{(\mathrm{g})}) = 1 - K_{\mathbf{s}}^{(\mathrm{g})}$. For the agent in Fig. 3e where $K_{\mathbf{s}}^{(\mathrm{g})} = 0$ and $F(0) = 1$, we have $\hat{P} = P$. In this configuration, there are 18 vacant sites in $\mathcal{N}_2$ and the probability of placing a daughter agent at the target site, highlighted in green, is $\hat{P}/18$. In Fig. 3f, where the agent at site $\mathbf{s}$ is surrounded by six neighbour agents, the probability of undergoing a birth event is $\hat{P} = 2P/3$, as $K_{\mathbf{s}}^{(\mathrm{g})} = 1/3$ and $F(1/3) = 2/3$. Since there are 12 vacant sites in $\mathcal{N}_2$, the probability of placing a daughter agent at the target site is $\hat{P}/12$. Similarly, in Fig. 3g, we have $\hat{P} = P/3$,

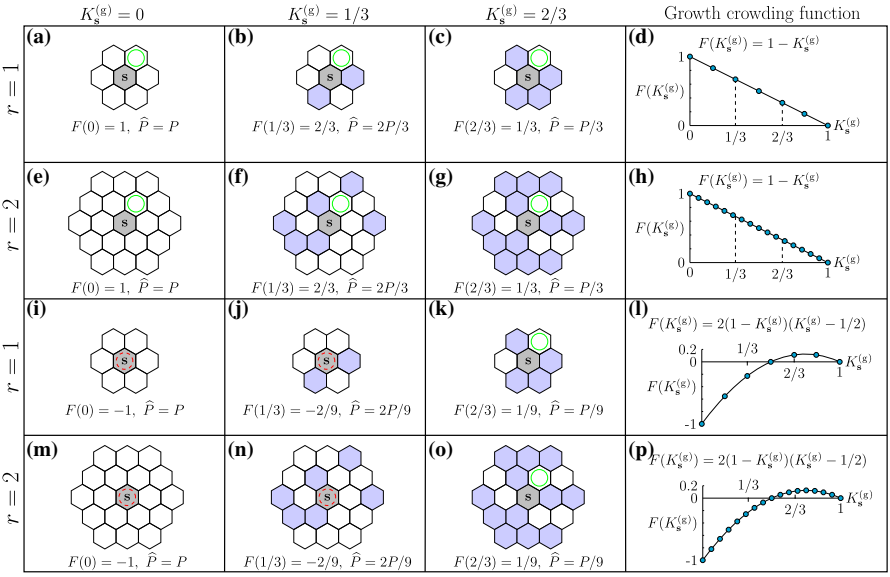

Fig. 3 Growth mechanisms with different-sized spatial templates and growth crowding functions. In each lattice fragment, site **s** is shaded grey, occupied sites within the template are shaded blue, and vacant sites within the template are unshaded (white). Each subfigure shows a potential outcome for an agent at site **s**. The crowdedness of $\mathcal{N}_1$ is shown in **a**–**c** and **i**–**k**. The crowdedness of $\mathcal{N}_2$ is shown in **e**–**g** and **m**–**o**. The agent at site **s** can undergo a birth event when $F > 0$ as in (a)–(c), (e)–(g), (k) and (o). In contrast, the agent at site **s** can undergo a death event when $F < 0$ as in **i**, **j**, **m** and **n**. The solid green circles represent the target site for the placement of a daughter agent during a successful proliferation event, and the dashed red circles indicate the location of agents that can undergo a death event (Color figure online)

as $K_s^{(g)} = 2/3$ and $F(2/3) = 1/3$. The probability of placing a daughter agent at the target site is $\hat{P}/6$. All results in Fig. 3a–h consider the simplest linear crowding function $F(K_s^{(g)}) = 1 - K_s^{(g)}$, which means that agents do not die in this case, since $F(K_s^{(g)}) \geq 0$.

We now choose a nonlinear growth crowding function $F(K_s^{(g)}) = 2(1 - K_s^{(g)})(K_s^{(g)} - 1/2)$ that can take on both positive and negative values, as shown in Fig. 3l. In this case, we make a distinction between a birth event when $F(K_s^{(g)}) > 0$, a death event when $F(K_s^{(g)}) < 0$, and no event when $F(K_s^{(g)}) = 0$. We first consider a nearest-neighbour template with $r = 1$ in Fig. 3i–k. In Fig. 3i, the agent at site **s** dies with probability $\hat{P} = P|F(K_s^{(g)})|$. Here, $K_s^{(g)} = 0$ and $F(0) = -1$, thus $\hat{P} = P$. In Fig. 3j, the agent at site **s** dies with probability $\hat{P} = 2P/9$ as $K_s^{(g)} = 1/3$ and $F(1/3) = -2/9$. In Fig. 3(k), the agent at site **s** undergoes a birth event with probability $\hat{P} = P/9$ as $K_s^{(g)} = 2/3$ and $F(2/3) = 1/9$. As there are two vacant sites in $\mathcal{N}_1$, the probability of placing a daughter agent at the target site is $\hat{P}/2$.

Finally, we consider a larger template with $\mathcal{N}_2$ in Fig. 3m–o. In Fig. 3m, the agent at site **s** dies with probability $\hat{P} = P|F(K_s^{(g)})|$, where $F(K_s^{(g)}) = 2(1 - K_s^{(g)})(K_s^{(g)} - 1/2)$. Here, $K_s^{(g)} = 0$ and $F(0) = -1$, thus $\hat{P} = P$. In Fig. 3n, the agent at site **s**

dies with probability $\hat{P} = 2P/9$ as $K_{\mathbf{s}}^{(\mathrm{g})} = 1/3$ and $F(1/3) = -2/9$. In Fig. 3o, the agent at site $\mathbf{s}$ undergoes a birth event with probability $\hat{P} = P/9$ as $K_{\mathbf{s}}^{(\mathrm{g})} = 2/3$ and $F(2/3) = 1/9$. As there are six vacant sites in $\mathcal{N}_2$, the probability of placing a daughter agent at the target site is $\hat{P}/6$.

The movement crowding function, $G(K_{\mathbf{s}}^{(\mathrm{m})})$, is incorporated into the model in a similar way as the growth crowding function except that it is always non-negative, $G(K_{\mathbf{s}}^{(\mathrm{m})}) \in [0, 1]$. In this section, we have sought to describe the discrete mechanism as clearly as possible with the use of Figs. 2 and 3. For the remainder of this work, we focus on results where we set $r = 1$ for movement and $r = 4$ for growth. Other choices of r can be implemented using the software available on GitHub.

3 Continuum Limit

In this section, we derive the mean-field continuum limit of the discrete model. The *averaged* occupancy of site $\mathbf{s}$, constructed from V identically prepared realisations of the discrete model, can be written as

$$\bar{C}_{\mathbf{s}} = \frac{1}{V} \sum_{v=1}^{V} C_{\mathbf{s}}^{(v)}(t), \tag{3}$$

where $C_{\mathbf{s}}^{(v)}(t) \in \{0, 1\}$ is the binary occupancy of site $\mathbf{s}$ at time t in the vth identically prepared realisation of the discrete model. We note that $\bar{C}_{\mathbf{s}} \in [0, 1]$ and is a function of time, t, but we suppress this dependence for notational convenience. Similarly, the *averaged* occupancy of $\mathcal{N}_r\{\mathbf{s}\}$, again constructed from V identically prepared realisations, is given by

$$\bar{K}_{\mathbf{s}}(r) = \frac{1}{|\mathcal{N}_r|} \sum_{\mathbf{s}' \in \mathcal{N}_r\{\mathbf{s}\}} \bar{C}_{\mathbf{s}'}. \tag{4}$$

As we use a nearest-neighbour template, $r = 1$, for movement, and a larger template, $r = 4$, for growth, we denote the averaged occupancy of sites for potential movement events as $\bar{K}_{\mathbf{s}}^{(\mathrm{m})}$, and the averaged occupancy of sites for potential growth events as $\bar{K}_{\mathbf{s}}^{(\mathrm{g})}$.

To arrive at an approximate continuum limit description, we start by writing down an expression for the expected change in occupancy of site $\mathbf{s}$ during the time interval from t to $t + \tau$,

$$\delta(\bar{C}_{\mathbf{s}}) = \overbrace{\frac{M}{|\mathcal{N}_1|}(1-\bar{C}_{\mathbf{s}})\sum_{\mathbf{s}'\in\mathcal{N}_1\{\mathbf{s}\}}\bar{C}_{\mathbf{s}'}\frac{G(\bar{K}^{(\mathrm{m})}_{\mathbf{s}'})}{1-\bar{K}^{(\mathrm{m})}_{\mathbf{s}'}}}^{\text{movement events into } \mathbf{s}} - \overbrace{M\bar{C}_{\mathbf{s}}G(\bar{K}^{(\mathrm{m})}_{\mathbf{s}})}^{\text{movement events out of } \mathbf{s}}$$
$$+ \underbrace{\frac{P}{|\mathcal{N}_4|}(1-\bar{C}_{\mathbf{s}})\sum_{\mathbf{s}'\in\mathcal{N}_4\{\mathbf{s}\}}\mathbb{H}(F(\bar{K}^{(\mathrm{g})}_{\mathbf{s}'}))\bar{C}_{\mathbf{s}'}\frac{F(\bar{K}^{(\mathrm{g})}_{\mathbf{s}'})}{1-\bar{K}^{(\mathrm{g})}_{\mathbf{s}'}}}_{\text{birth events: place new agents onto } \mathbf{s}} \tag{5}$$
$$- \underbrace{(1-\mathbb{H}(F(\bar{K}^{(\mathrm{g})}_{\mathbf{s}}))P\bar{C}_{\mathbf{s}}F(\bar{K}^{(\mathrm{g})}_{\mathbf{s}})}_{\text{death events: remove agent from } \mathbf{s}},$$

where $\mathbb{H}$ is the Heaviside step function. Each term in Eq. (5) has a relatively simple physical interpretation. The first term on the right hand side of Eq. (5) represents the change in occupancy of site $\mathbf{s}$ owing to the expected movement of agents in $\mathcal{N}_1\{\mathbf{s}\}$ into site $\mathbf{s}$. The factor $1/(1-\bar{K}^{(\mathrm{m})}_{\mathbf{s}})$ accounts for the choice of the target site in $\mathcal{N}_1$ being randomly selected from the available vacant sites. The second term on the right hand side of Eq. (5) represents the change in occupancy of site $\mathbf{s}$ owing to the expected movement of agents out of site $\mathbf{s}$. The third term on the right hand side of Eq. (5) represents the change in occupancy owing to the expected birth events of agents in $\mathcal{N}_4\{\mathbf{s}\}$ that would place daughter agents onto site $\mathbf{s}$, where $F(\bar{K}^{(\mathrm{g})}_{\mathbf{s}}) > 0$. Again, the factor $1/(1-\bar{K}^{(\mathrm{g})}_{\mathbf{s}})$ accounts for the choice of the target site in $\mathcal{N}_4$ being randomly selected from the available vacant sites. The last term on the right hand side of Eq. (5) represents the expected change in occupancy owing to agent death at site $\mathbf{s}$, when $F(\bar{K}^{(\mathrm{g})}_{\mathbf{s}}) < 0$. Note that this approximate conservation statement (5) makes use of the mean-field assumption, whereby the occupancy status of lattice sites is taken to be independent (Baker and Simpson 2010).

To derive the continuum limit, we replace $\bar{C}_{\mathbf{s}}$ with a continuous function, $C(x, y, t)$, and expand each term in Eq. (5) in a Taylor series about site $\mathbf{s}$, and truncate terms of $\mathcal{O}(\Delta^3)$. Subsequently, we divide both sides of the resulting expression by τ and evaluate the resulting expressions in the limit $\Delta \to 0$ and $\tau \to 0$ jointly, with the ratio of Δ^2/τ held constant (Hughes 1995). This leads to the following nonlinear RDE,

$$\frac{\partial C(x,y,t)}{\partial t} = D_0\nabla\cdot(D(C)\nabla C(x,y,t)) + \lambda C(x,y,t)F(C), \tag{6}$$

where

$$D(C) = C\frac{\mathrm{d}G(C)}{\mathrm{d}C} + \frac{1+C}{1-C}G(C), \tag{7}$$

and

$$D_0 = \frac{M}{4}\lim_{\Delta,\tau\to 0}\frac{\Delta^2}{\tau}, \quad \lambda = \lim_{\tau\to 0}\frac{P}{\tau}. \tag{8}$$

Here, D_0 is the free-agent diffusivity, $D(C)$ is a nonlinear diffusivity function that relates to the movement crowding function $G(C)$, and λ is the rate coefficient associated with the source term that is related to the growth crowding function $F(C)$. To obtain a well-defined continuum limit, we require that $P = \mathcal{O}(\tau)$ (Simpson et al. 2010). The algebraic details required to arrive at the continuum limit are outlined in the Supplementary Material.

For all simulations in this work, we use $\Delta = \tau = 1$, giving $D_0 = M/4$ and $\lambda = P$. This is equivalent to working in a non-dimensional framework (Simpson et al. 2010). If the model is to be applied to a particular dimensional problem, then Δ and τ can be re-scaled using appropriate length and time scales. In this non-dimensional framework with $\tau = 1$, we satisfy the requirement that $P = \mathcal{O}(\tau)$ by ensuring $P/M \ll 1$. The main focus of this work is on the role of the growth mechanism, and the question of whether the population survives or goes extinct. We therefore set $G(C) = 1 - C$ leading to $D(C) = 1$. This means that the nonlinear diffusion term in Eq. (6) simplifies to a linear diffusion term, giving

$$\frac{\partial C(x, y, t)}{\partial t} = D_0 \nabla^2 C(x, y, t) + \lambda C(x, y, t) F(C). \tag{9}$$

We note that Eq. (9) has been studied extensively in applications involving the spatial spread of invasive species, such as the works of Fisher (1937); Skellam (1951); Fife (1979); Lewis and Kareiva (1993) and Hastings et al. (2005). Some previous models consider a logistic-type source term (Fisher 1937), while others consider Allee-type bistable source term (Sewalt et al. 2016). Under these conditions, many results have been established. For example, if we consider Eq. (9) on a one-dimensional infinite domain, it is well known that this model supports travelling wave solutions for both logistic (Fisher 1937) and bistable (Fife 1979) source terms. In this work, however, we take a different perspective by studying Eq. (9) on a finite domain and so the question of analysing travelling wave solutions is not our focus. Moreover, although Lewis and Kareiva (1993) give a critical radius of a radially symmetric distribution so that the initial distribution converges to an expanding wave in an infinite domain, their analysis is valid under the assumption that the time scale of growth is much faster than the time scale of migration, which corresponds to $P/M \gg 1$ in our framework. Our discrete model does not have any such restriction and can be implemented for any $M \in [0, 1]$ and any $P \in [0, 1]$. In contrast, our continuum model requires $P/M \ll 1$ to correspond to the discrete model, and we will explore the consequences of these differences in our results.

In the rest of this work, we choose

$$F(C) = a(1 - C)(C - A), \quad \text{with} \quad a = \frac{5}{2}, \quad A = \frac{2}{5}, \tag{10}$$

since this leads to the canonical cubic source term $\lambda C F(C)$ associated with Allee kinetics. In particular, we set $A = 2/5$ so that this choice of $F(C)$ can be used to represent birth events where $C > 2/5$ and death events where $C < 2/5$, see Fig. 4d. We further set $a = 5/2$ leading to $F(0) = -1$, so that attempted death events for an isolated agent, where $C = 0$, are always successful.

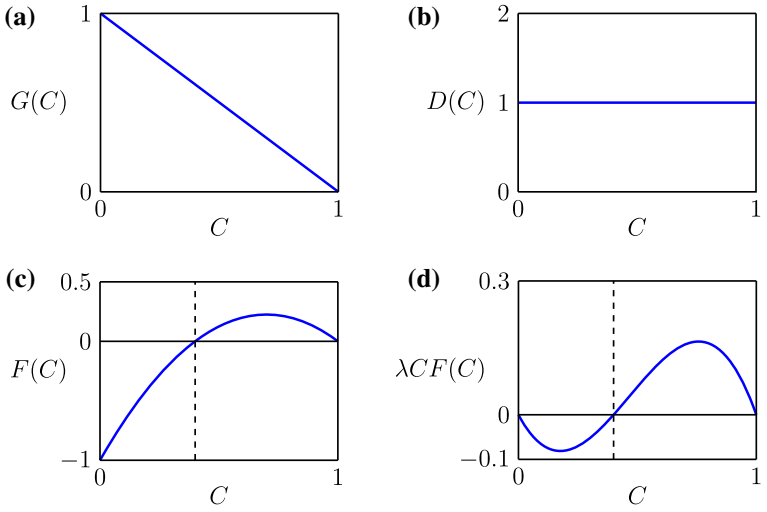

Fig. 4 Specific crowding functions used in this work. **a–b** Setting $G(C) = 1-C$ for the movement crowding function leads to linear diffusion, $D(C) = 1$. **c–d** Setting $F(C) = 5(1-C)(C-2/5)/2$ for the growth crowding function with $\lambda = P = 1$ leads to $\lambda C F(C) = 5C(1-C)(C-2/5)/2$. The dashed lines in (**c–d**) relate to the Allee threshold, $A = 2/5$

In summary, our discrete model requires the specification of two crowding functions: $G(C)$ and $F(C)$. These crowding functions are related to macroscopic quantities in the associated RDE model. In particular, $G(C)$ is related to a nonlinear diffusivity function, $D(C)$, and $F(C)$ is related to a nonlinear source term $\lambda C F(C)$. Figure 4 shows the relationship between these functions for our choice of $G(C)$ and $F(C)$.

4 Initial Distributions and Simulation Data

In this section, we consider the three initial distributions shown in Fig. 1 with $L = 100$, and we introduce the corresponding continuous descriptions. In general, each of the initial distribution shown in Fig. 1 can be written as

$$C(x, y, 0) = \begin{cases} B, & (x, y) \in \mathcal{H}, \\ 0, & \text{elsewhere}, \end{cases} \tag{11}$$

where $\mathcal{H}$ is the region in which individuals are distributed at density $B \in (0, 1]$. For the discrete model, we randomly distribute a fixed number of agents on $\mathcal{H}$ so that the averaged density across $\mathcal{H}$ is B. For example, all agents in the discrete model are closely packed together if $B = 1$. In contrast, for the continuum model, the density is B at each position in $\mathcal{H}$.

For the three initial distributions in Fig. 1, we will report data from the stochastic model in the following way. We denote the averaged occupancy of site $\mathbf{s}$ in V identically prepared simulations as

$$\langle C(x, y, t)\rangle = \frac{1}{V}\sum_{v=1}^{V} C^{(v)}(i, j, n), \tag{12}$$

where we note that the average denoted by the angular parenthesis is taken in the same way as the average in Eq. (3). Here, site $\mathbf{s}$, indexed by i and j, are related to position, (x, y) via Eq. (1). The averaged occupancy $\langle C(x, y, t)\rangle$ is a measure of the local density at location (x, y), and time $t = n\tau$ after the nth time step in the stochastic discrete model. Although (12) describes the averaged occupancy of any distribution, there are more concise forms for the vertical strip distributions in Fig. 1b. As the initial occupancy is independent of the vertical position, we denote the averaged occupancy of any site as

$$\langle C(x, t)\rangle = \frac{1}{VJ}\sum_{v=1}^{V}\sum_{j=1}^{J} C^{(v)}(i, j, n), \tag{13}$$

which is a measure of the density at location x and at time $t = n\tau$. Note that, as we will show through simulation, the density of agents remains independent of the vertical position for all $t > 0$ because we use periodic boundary conditions. Similarly, for simulations relating to the well-mixed initial distribution as in Fig. 1a, where the initial density is independent of position, we denote the averaged occupancy of any site as

$$\langle C(t)\rangle = \frac{1}{VIJ}\sum_{v=1}^{V}\sum_{j=1}^{J}\sum_{i=1}^{I} C^{(v)}(i, j, n), \tag{14}$$

which is a measure of the total population density at time $t = n\tau$. As we will show through simulation, in this case the density of agents remains independent of position for all $t > 0$. The total population density $\langle C(t)\rangle$ is also useful to describe simulations starting from the square and vertical strip initial distributions. In summary, data from the discrete models can be summarised by calculating $\langle C(x, y, t)\rangle$, $\langle C(x, t)\rangle$, and $\langle C(t)\rangle$.

For the well-mixed initial distribution, as shown in Fig. 1a, Eq. (9) simplifies to

$$\frac{\mathrm{d}C(t)}{\mathrm{d}t} = \lambda C(t)F(C), \tag{15}$$

where $C(t)$ represents the total density of the population (Simpson et al. 2010). This separable ODE can be solved to give an implicit solution for our choice of $F(C)$.

For the vertical strip initial distribution, as shown in Fig. 1b, Eq. (9) simplifies to

$$\frac{\partial C(x,t)}{\partial t} = D_0 \frac{\partial^2 C(x,t)}{\partial x^2} + \lambda C(x,t) F(C), \tag{16}$$

where $C(x,t)$ represents the column-averaged density of agents (Simpson et al. 2010). An extensive discussion and exploration of the implications of simplifying the two-dimensional nonlinear RDE into this simpler one-dimensional RDE is given in Simpson (2009). Given a numerical solution of Eq. (16), as outlined in the Supplementary Material, we compute

$$\mathcal{C}(t) = \frac{1}{L} \int_0^L C(x,t)\, \mathrm{d}x, \tag{17}$$

which is the total density of the population in the whole domain and corresponds to $\langle C(t) \rangle$ in the discrete model.

For the square initial distribution, to compare averaged data from the discrete model with the solution of the continuum model we solve Eq. (9) numerically to give $C(x, y, t)$. Full details of the numerical methods are presented in the Supplementary Material. Using the numerical solution for $C(x, y, t)$, we calculate

$$\mathcal{C}(t) = \frac{1}{L^2} \int_0^L \int_0^L C(x,y,t)\, \mathrm{d}x\, \mathrm{d}y, \tag{18}$$

which, again, is the total density of the population in the whole domain.

We now show the evolution of the total population density in both the discrete and continuum models with these three initial distributions. Setting all three initial distributions with $\mathcal{C}(0) = 0.25$ and considering $P/M = 1/1000$ or $P/M = 8/1000$, representing two kinds of populations with different ratios of time scale of migration and growth, we show $\mathcal{C}(t)$ and $\langle C(t) \rangle$ in Fig. 5, where we calculate $\langle C(t) \rangle$ with 40 identically prepared realisations. In all cases, the continuum model accurately captures the averaged data from the discrete model. The well-mixed initial distribution leads to population survival with both $P/M = 1/1000$ and $P = 8/1000$, whereas the vertical strip and square initial distributions lead to population extinction when $P/M = 1/1000$, but population survival when $P/M = 8/1000$, as shown in Fig. 5e–f and Fig. 5h–i. This is interesting as the global density averaged across the whole domain is smaller than the Allee threshold. This comparison indicates that the vertical strip and square initial distributions may sometimes lead to the survival of the population, whereas the same initial number of individuals in a well-mixed environment would lead to extinction. These differences are due to the interplay between the role of the initial spatial distribution and the ratio of time scale of migration to the time scale of proliferation and death. Additional results in the Supplementary Material provide more detailed comparisons of the solutions of the continuum model and appropriately averaged data from the discrete model. Additional results relating to the robustness of the averaged data is also explored in the Supplementary Material. Overall, the numerical solution of the continuum model provides a useful way of accurately studying

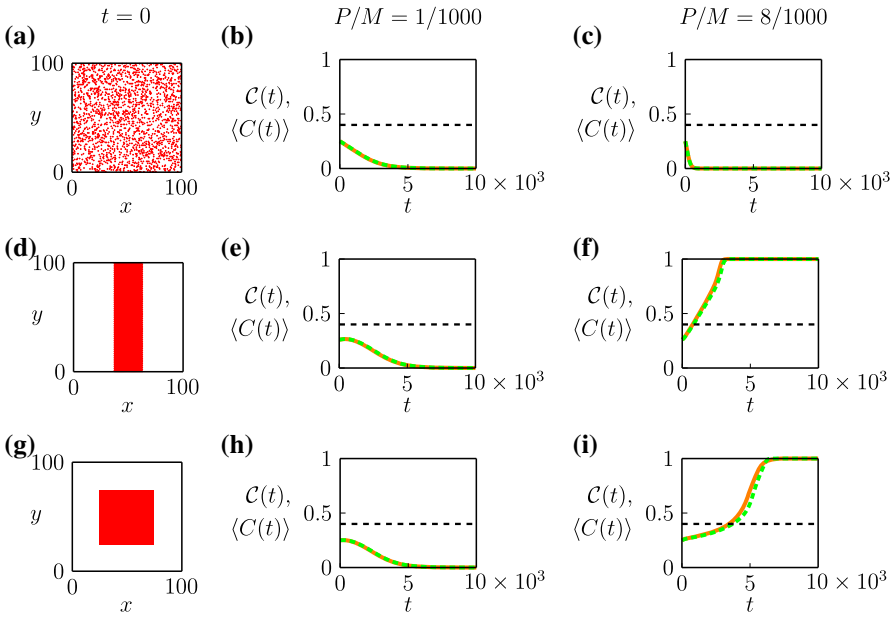

Fig. 5 The ratio P/M and the shape of the initial spatial distribution influence the fate of populations. **a** Well-mixed initial distribution with $B = 0.25$ leading to $\mathcal{C}(0) = 0.25$. **b** $\langle C(t)\rangle$ (solid orange) and $\mathcal{C}(t)$ (dashed green) for the well-mixed initial distribution with $P/M = 1/1000$. **c** $\langle C(t)\rangle$ (solid orange) and $\mathcal{C}(t)$ (dashed green) for the well-mixed initial distribution with $P/M = 8/1000$. **d** Vertical strip initial distribution with width $w_1 = 25$ leading to $\mathcal{C}(0) = 0.25$. **e** $\langle C(t)\rangle$ (solid orange) and $\mathcal{C}(t)$ (dashed green) for the vertical strip initial distribution with $P/M = 1/1000$. **f** $\langle C(t)\rangle$ (solid orange) and $\mathcal{C}(t)$ (dashed green) for the vertical strip initial distribution with $P/M = 8/1000$. **g** Square initial distribution with width $w_1 = 50$ leading to $\mathcal{C}(0) = 0.25$. **h** $\langle C(t)\rangle$ (solid orange) and $\mathcal{C}(t)$ (dashed green) for the square initial distribution with $P/M = 1/1000$. **i** $\langle C(t)\rangle$ (solid orange) and $\mathcal{C}(t)$ (dashed green) for the square initial distribution with $P/M = 8/1000$. The dashed black horizontal lines in (b)–(c), (e)–(f) and (h)–(i) indicate the Allee threshold, $A = 0.4$ (Color figure online)

the expected behaviour of the discrete model. Of interest is that the long-term fate of populations varies with the spatial arrangement of the initial distributions. Our aim now is to study these differences more carefully.

5 Role of the Shape of the Initial Distribution

In this section, we explore the influence of more complicated two-dimensional shapes of the initial distribution on the fate of populations. Our results in Sect. 4 indicate that several factors are at play when we consider the long-term fate of bistable populations. First, the spatial arrangement of the initial population plays an important role. Second, the ratio P/M also influences the fate of populations. Since the initial distribution of the population is given by Eq. (11), the initial distribution varies with both B and the size of the initially occupied region $\mathcal{H}$ except that the well-mixed initial distribution only varies with B. In the remainder of the main document, we fix $B = 1$ and alter the initial population size by adjusting the size of $\mathcal{H}$ for the initial distributions that are not

well-mixed. Additional results in the Supplementary Material indicate that varying B does not change our overall observations and conclusions.

To systematically study the transition between population extinction to population survival, we take the $(\mathcal{C}(0), P/M)$ phase space and discretise it uniformly into a rectangular mesh, with 51×40 nodes in Fig. 6n. We vary $\mathcal{C}(0)$ by changing B in the well-mixed initial distribution, whereas we vary $\mathcal{C}(0)$ by changing the size of $\mathcal{H}$ in the vertical strip and square initial distributions as shown in Figures 6a–c and Fig. 6d–f, respectively. We also vary the ratio P/M by holding $M = 1$ and choosing $P \in [1/1000, 4/100]$ in the discrete model. As $P/M = \lambda/(4D_0)$, we hold $D_0 = 1/4$ and vary λ in the continuum model. With each pair of parameters, we run the numerical simulation of the continuum model after a sufficiently long period of time so that the population either leads to survival or extinction. In Fig. 6n, we draw the survival/extinction thresholds from the continuum model with the well-mixed, vertical strip and square initial distributions. In the vertical strip and square cases, we see that the long-term survival is strongly dependent upon P/M whereas in the well-mixed initial distribution this dependence is less pronounced. Additional results in the Supplementary Material show the good agreement in the prediction of survival or extinction between the continuum and discrete models and further show the role of stochasticity in discrete simulations.

A key feature of the initial shape is the dimension of the shape. The well-mixed, vertical strip and square initial distributions can be thought of as zero-, one- and two-dimensional shapes, respectively. To highlight the influence of the dimensionality on the fate of the population, we consider a rectangular distribution of varying initial heights, see Fig. 6g–i. The initially occupied region $\mathcal{H}$ is a rectangle with width $w_1 = 40$ and height $w_2 \in [25, 100]$, which leads to $\mathcal{C}(0) \in [0.1, 0.4]$. When $\mathcal{C}(0) = 0.16$ with $w_2 = 40$, the rectangular initial distribution is the same as the square initial distribution, as shown in Fig. 6e and (h). When $\mathcal{C}(0) = 0.4$ with $w_2 = 100$, the rectangular initial distribution is the same as the vertical strip initial distribution, as shown in Fig. 6c and i. Note that we use $\mathcal{C}(0)$ as the horizontal axis in the phase diagram so that we can compare the results with different shapes of initial distributions. We show the evolution of the total population density in the continuum model with $M = 1$ and $P = 0.0028$, leading to $D_0 = 1/4$ and $\lambda = 0.0028$, and different $\mathcal{C}(0)$ in Fig. 6j–m. When $\mathcal{C}(0) = 0.2$ and $\mathcal{C}(0) = 0.3$, the rectangular initial distribution leads to extinction, which is the same as the results obtained from the square initial distribution. While the vertical strip initial distribution leads to survival with $\mathcal{C}(0) = 0.3$. In contrast, when $\mathcal{C}(0) = 0.33$ and $\mathcal{C}(0) = 0.36$, the rectangular initial distribution leads to survival, which is the same as the results obtained from the vertical strip initial distribution. While the square initial distribution leads to extinction with $\mathcal{C}(0) = 0.33$. This indicates a switch of the influence of the rectangular initial distribution on the fate of populations from a manner similar to the square initial distribution to a manner similar to the vertical strip initial distribution. In Fig. 6n, we draw the survival/extinction boundary from the continuum model with the rectangular initial distribution in the $(\mathcal{C}(0), P/M)$ phase space for $\mathcal{C}(0) \in [0.1, 0.4]$ and $P/M = [1/10000, 21/1000]$ and compare them to the results obtained from the vertical strip initial distribution and from the square initial distribution. Although the results are from the continuum model, we still use P/M as the vertical axis to reflect the connection between the

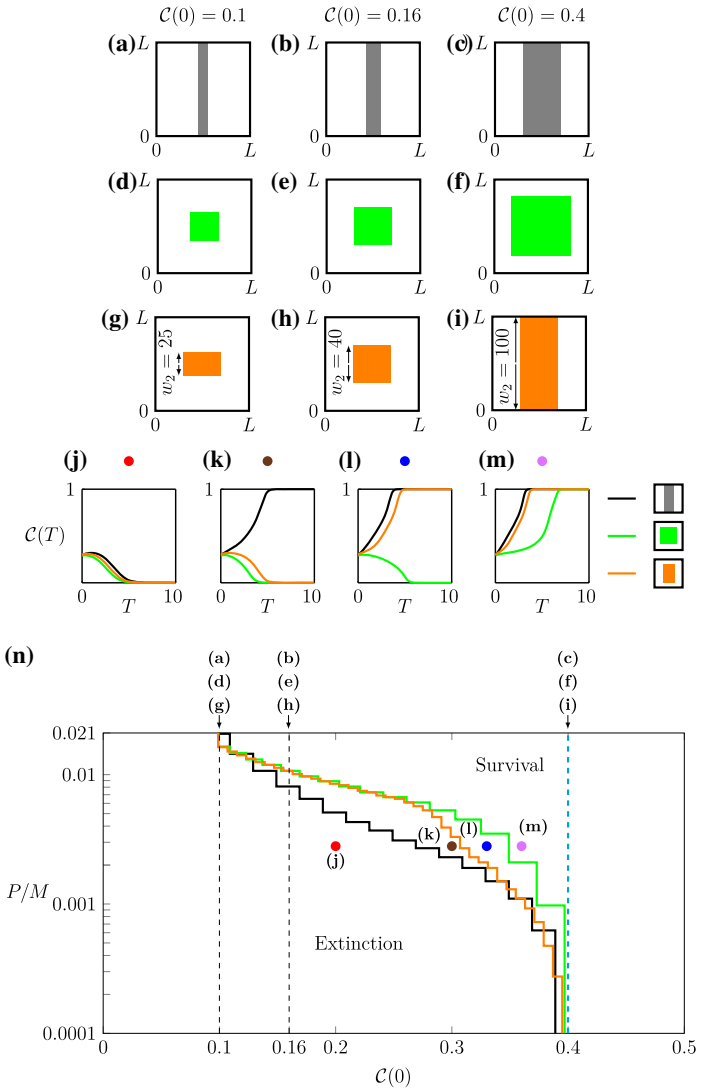

Fig. 6 Influence of dimensionality in rectangular initial distributions. **a–c** Vertical strip (one-dimensional) initial distributions varied with the width $w_1 \in [10, 40]$. **d–f** Square (two-dimensional) initial distributions varied with the width $w_1 \in [32, 64]$. **g–i** The rectangular initial distributions varied with the height $w_2 \in [25, 100]$ with a fixed width $w_1 = 40$. **j–m** The evolution of the total population density $\mathcal{C}(T)$ where $T = 10^3 t$ with $P/M = 0.0028$, $\mathcal{C}(0) = 0.2$ in (**j**), 0.3 in (**k**), 0.33 in (**l**) and 0.36 in (**m**), and with the vertical strip (black), square (green) and rectangular (orange) initial distributions. **n** Phase diagram showing the survival/extinction boundaries constructed from a 151×120 array of $\mathcal{C}(0) \in [1/10, 1/40]$ and $P/M \in [1/10000, 21/1000]$. Three curves indicate the survival/extinction thresholds from the continuum model of the vertical strip (black), square (green) and rectangular (orange) initial distributions. Three dashed lines represent $\mathcal{C}(0) = 0.1, 0.16$ and 0.4, where $\mathcal{C}(0) = 0.4$ (cyan) is also the survival/extinction threshold of the well-mixed initial distributions. Note that we use a logarithmic scale for the P/M axis (Color figure online)

discrete and continuum models in our framework. We observe that there is a clear transition of the survival/extinction boundary for the rectangular initial distribution. The survival/extinction boundary of the rectangular initial distribution is close to the survival/extinction boundary obtained from the square initial distribution when $\mathcal{C}(0)$ is small and is close to the survival/extinction boundary obtained from the vertical strip initial distribution when $\mathcal{C}(0)$ is large. This transition indicates that the dimensionality of the initial shape of a population plays a role in determining the ultimate fate of the population.

Many more spatial arrangements of the population can be considered. We first consider a circle with radius r as the initially occupied region $\mathcal{H}$, as shown in Fig. 7a. We draw the phase diagram on the $(\mathcal{S}, P/M)$ space, where $\mathcal{S}$ denotes the area of the initially occupied region $\mathcal{H}$, from the continuum model with $L = 100$ by varying $P/M \in [1/1000, 21/1000]$ where $M = 1$ and $\mathcal{S} = \pi r^2 \in [1000, 5000]$ with $r \in [17.8, 39.9]$ in Fig. 7b. We then consider the critical initial radius

$$r_{\text{crit}} = \sqrt{\frac{2D_0}{\lambda a}} \frac{1}{1-2A}, \tag{19}$$

derived by Lewis and Kareiva (1993), which leads to the critical initial area $\mathcal{S}_{\text{crit}} = \pi r_{\text{crit}}^2$. As λ and D_0 depend on P and M in our framework, we derive the survival/extinction threshold of the initial area

$$\mathcal{S}_{\text{crit}} = \frac{\pi M}{2aP} \frac{1}{(1-2A)^2}, \tag{20}$$

and draw the extinction/survival boundary in the $(\mathcal{S}, P/M)$ phase space based on (20) in Fig. 7b. Although the critical initial radius is formally derived in the limit $P/M \gg 1$, this result also appears to work well here where P/M is not that large. We now consider a larger domain with $L = 200$ in Fig. 7c, in this case the match between the survival/extinction boundary of the circular initial distribution and the critical initial area is better because the role of boundaries becomes less important. Furthermore, we compare the survival/extinction boundary to the result obtained from the square initial distribution with $L = 100$ and $L = 200$ in Figs. 7b and c, respectively. Note that in the square initial distribution the area of $\mathcal{H}$ is given by $\mathcal{S} = w_1^2$. The survival/extinction boundaries obtained with the circular and square initial distributions are very close, which indicates that these two initial distributions give rise to similar outcomes. This could be attributed to the fact that they are both compact initial distributions with a small perimeter to area ratio.

A natural question is whether populations with other two-dimensional initial distributions have the similar critical initial area determined by (19). To explore this, we now consider a square annulus in the middle of the domain as the initially occupied region, as shown in Fig. 8a. The area of the region is determined by a fixed outer width $w_1 = 64$ and a variable inner width w_2. We also consider a circle as the initially occupied region, as shown in Fig. 8b. The area of the region varies with radius r. We show the evolution of the total population density in the continuum model with these two initial shapes at $P/M = 0.01$, where $M = 1$ and $P = 0.01$ leading to $D_0 = 1/4$ and

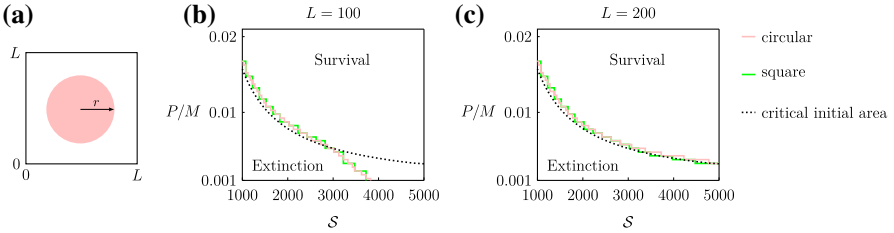

Fig. 7 Phase diagram for survival/extinction with the circular initial distributions. **a** A circular initial distribution with radius r. **b, c** Phase diagrams on a rectangular mesh with 81×41 nodes for $\mathcal{S} \in [0.1, 0.5]$ and $P/M \in [1/1000, 21/1000]$ where $M = 1$. We consider $L = 100$ in (b) and $L = 200$ in (c). Pink curves indicate the survival/extinction thresholds in the continuum model with the circular initial distributions. Green curves indicate the survival/extinction thresholds in the continuum model with the square initial distributions. Black dotted curves indicate the survival/extinction thresholds obtained from (20) (Color figure online)

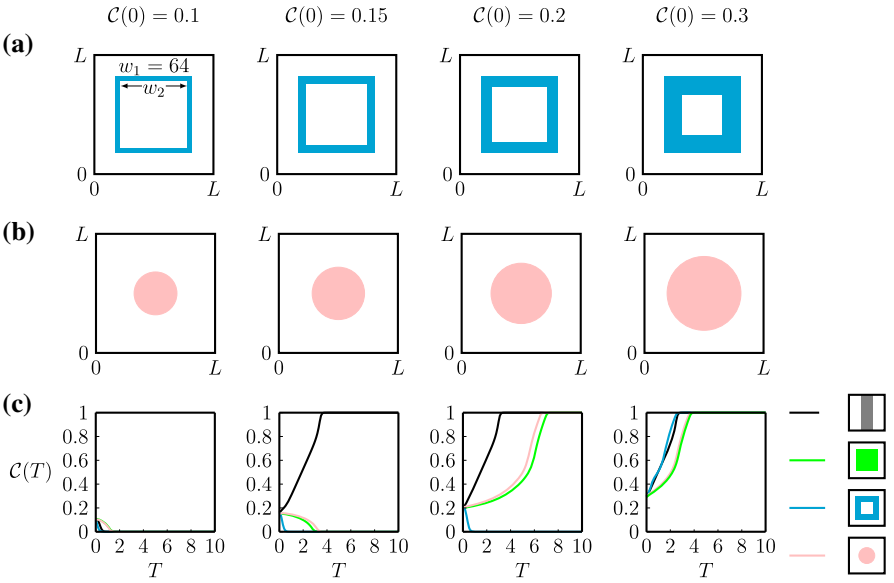

Fig. 8 Population dynamics with more complicated initial spatial distributions. **a** Square annular initial distributions with a fixed outer width $w_1 = 64$ and different values of inner width w_2. **b** Circular initial distributions with different values of radius r. **c** The evolution of the total population density $\mathcal{C}(T)$ which considers $T = \lambda t$, $P/M = 0.01$ with $P = 0.01$ and $M = 1$ leading to $\lambda = 0.01$ and $D_0 = 1/4$, and $\mathcal{C}(0) = 0.1, 0.15, 0.2, 0.3$ with different initial distributions. Black curves are generated by the vertical strip initial distributions. Green curves are generated by the square initial distributions. Cyan curves are generated by the square annular initial distributions. Pink curves are generated by the circular initial distributions (Color figure online)

$\lambda = 0.01$, and different $\mathcal{C}(0)$. We further show the results obtained from the vertical strip initial distributions and the square initial distributions in Fig. 8c. All four initial distributions lead to population extinction when $\mathcal{C}(0) = 0.1$. When $\mathcal{C}(0) = 0.15$, only the vertical strip initial distribution leads to population survival. When $\mathcal{C}(0) = 0.2$, the square and circular initial distributions also lead to population survival. In contrast,

the square annular initial distribution still leads to population extinction. Note that $P/M = 0.01$ leads to $A_{\text{crit}} \approx 1570$ and $\mathcal{C}(0)_{\text{crit}} = 0.157 < 0.2$. This suggests that, although the area of the square annulus exceeds the critical initial area given in Lewis and Kareiva (1993), it still leads to population extinction. When $\mathcal{C}(0) = 0.3$, all four initial distributions lead to population survival. These results indicate that, although some initial distributions have the same area of the initially occupied region, they may lead to different fates of the population. It is the shape of the initially occupied region that dictates whether a bistable population survives or goes extinct. This suggests the importance of considering the influence of the spatial arrangements of individuals on the long-term survival of populations.

6 Conclusions and Outlook

In this work, we design, analyse and implement a new two-dimensional stochastic discrete model incorporating movement, birth and death events with crowding effects to study population extinction. The continuum limit of the discrete model is a nonlinear RDE which can be used to study a wide range of macroscopic phenomena including linear diffusion, nonlinear diffusion, as well as logistic and bistable growth kinetics. Since the aim of this work is to focus on long-term survival or extinction, we choose the movement crowding function to be $G(C) = 1 - C$ which corresponds to macroscopic linear diffusion. In addition, we choose the growth crowding function to be $F(C) = a(1 - C)(C - A)$ which leads to a classical cubic bistable source term with Allee threshold A.

The focus of our work is to use the discrete and continuum models to explore the factors that influence the long-term fate of the bistable population. In particular, we explore different spatial arrangements of the population on a finite $L \times L$ domain with periodic boundary conditions. The well-mixed initial distribution involves distributing agents evenly across the entire $L \times L$ domain, the vertical strip initial distribution involves distributing agents along a vertical strip within the $L \times L$ domain so that the initial density is independent of vertical position in the domain, and the two-dimensional initial distributions involve distributing agents in a square, circular, rectangular or square annular region within the $L \times L$ domain. Our results show that the shape of initial distributions plays an important role in determining the fate of populations. This suggests the importance of considering the influence of spatial arrangements of individuals in studies of population dynamics.

There are many avenues for extending the work presented in this study. The stochastic model provides very detailed information including the age structure of the population and individual trajectories, see the results in the Supplementary Material. Furthermore, other shapes of initial distributions than those investigated here can be considered and similar numerical explorations of the long-term survival or extinction of the populations can be conducted using the software provided on GitHub for both the continuum and discrete models. Another feature of this work that could be explored is the choice of crowding functions. As we pointed out, all simulations here focus on $G(C) = 1 - C$, which gives rise to linear diffusion, and $F(C) = a(1 - C)(C - A)$ which gives rise to the classical cubic bistable term. Other choices of $G(C)$ and $F(C)$

can be incorporated into the discrete model to explore how the results presented here depend upon the precise details of these choices of crowding functions. We note that other choices of $G(C)$ lead to different motility mechanisms that are associated with nonlinear diffusion mechanisms, and that these can be important for applications where adhesion (Deroulers et al. 2009) and inertial effects (Zhang et al. 2019) are relevant. While we have not explicitly explored these effects in this work, our framework is sufficiently general that these mechanisms can be incorporated and explored, if required. Moreover, other boundary conditions could be incorporated in our model. In the Supplementary Material, we show that no-flux boundary conditions lead to the same result as when we consider periodic boundary conditions with symmetric rectangular initial distributions, while homogeneous Dirichlet boundary conditions only lead to the same result when the initial area is small. Furthermore, if we consider an asymmetric initial distribution, these three boundary conditions lead to different outcomes. Another interesting extension would be to consider Allee-type dynamics with populations of interacting species (Simpson et al. 2009a). Under these conditions, interactions can also contribute to the eventual survival or extinction of any of the subpopulations (Taylor et al. 2020; Krause and Van Gorder 2020).

Acknowledgements This work is supported by the Australian Research Council (DP200100177, DE200100988, DP190102545). We thank the two referees and the handling editor for their helpful suggestions.

References

Allee WC, Bowen ES (1932) Studies in animal aggregations: Mass protection against colloidal silver among goldfishes. J Exp Zool 61(2):185–207

Arroyo-Esquivel J, Hastings A (2020) Spatial dynamics and spread of ecosystem engineers: two patch analysis. Bull Math Biol 82(12):149

Baker RE, Simpson MJ (2010) Correcting mean-field approximations for birth-death-movement processes. Phys Rev E 82:041905

Böttger K, Hatzikirou H, Voss-Böhme A, Cavalcanti-Adam EA, Herrero MA, Deutsch A (2015) An emerging Allee effect is critical for tumor initiation and persistence. PLoS Comput Biol 11(9):e1004366

Bradford E, Philip JR (1970) Stability of steady distributions of asocial populations dispersing in one dimension. J Theor Biol 29(1):13–26

Bradford E, Philip JR (1970) Note on asocial populations dispersing in two dimensions. J Theor Biol 29(1):27–33

Chaplain MAJ, Lorenzi T, Macfarlane FR (2020) Bridging the gap between individual-based and continuum models of growing cell populations. J Math Biol 80(1):343–371

Courchamp F, Clutton-Brock T, Grenfell B (1999) Inverse density dependence and the Allee effect. Trend Ecol Evol 14(10):405–410

Courchamp F, Berec L, Gascoigne J (2008) Allee effects in ecology and conservation. Oxford University Press, Oxford

Deroulers C, Aubert M, Badoual M, Grammaticos B (2009) Modeling tumor cell migration: from microscopic to macroscopic models. Phys Rev E 79:031917

Drake JM (2004) Allee effects and the risk of biological invasion. Risk Anal 24(4):795–802

Druckenbrod NR, Epstein ML (2005) The pattern of neural crest advance in the cecum and colon. Dev Biol 287(1):125–133

Edelstein-Keshet L (2005) Mathematical models in biology. SIAM, Philadelphia

Etienne R, Wertheim B, Hemerik L, Schneider P, Powell J (2002) The interaction between dispersal, the Allee effect and scramble competition affects population dynamics. Ecol Model 148(2):153–168

Fadai NT, Simpson MJ (2020) Population dynamics with threshold effects give rise to a diverse family of Allee effects. Bull Math Biol 82(6):74
Fadai NT, Johnston ST, Simpson MJ (2020) Unpacking the Allee effect: determining individual-level mechanisms that drive global population dynamics. Proc Royal Soc A: Math, Phys Eng Sci 476(2241):20200350
Fife PC (1979) Long time behavior of solutions of bistable nonlinear diffusion equationsn. Arch Ration Mech Anal 70(1):31–36
Fisher RA (1937) The wave of advance of advantageous genes. Ann Eugen 7(4):355–369
Grindrod P (1996) The theory and applications of reaction-diffusion equations: patterns and waves. Clarendon Press, UK
Hastings A, Cuddington K, Davies KF, Dugaw CJ, Elmendorf S, Freestone A, Harrison S, Holland M, Lambrinos J, Malvadkar U, Melbourne BA, Moore K, Taylor C, Thomson D (2005) The spatial spread of invasions: new developments in theory and evidence. Ecol Lett 8(1):91–101
Holmes EE, Lewis MA, Banks JE, Veit RR (1994) Partial differential equations in ecology: spatial interactions and population dynamics. Ecology 75(1):17–29
Hughes BD (1995) Random walks and random environments: random walks, vol 1. Oxford University Press, Oxford
Jin W, Penington CJ, McCue SW, Simpson MJ (2016) Stochastic simulation tools and continuum models for describing two-dimensional collective cell spreading with universal growth functions. Phys Biol 13(5):056003
Johnston ST, Baker RE, McElwain DLS, Simpson MJ (2017) Co-operation, competition and crowding: a discrete framework linking Allee kinetics, nonlinear diffusion, shocks and sharp-fronted travelling waves. Sci Rep 7(1):42134
Kot M (2001) Elements of mathematical ecology. Cambridge University Press, Cambridge
Kot M, Lewis MA, van den Driessche P (1996) Dispersal data and the spread of invading organisms. Ecology 77(7):2027–2042
Krause AL, Van Gorder RA (2020) A non-local cross-diffusion model of population dynamics II: exact, approximate, and numerical traveling waves in single- and multi-species populations. Bull Math Biol 82(8):113
Lewis MA, Kareiva P (1993) Allee dynamics and the spread of invading organisms. Theor Popul Biol 43(2):141–158
Lewis MA, Petrovskii SV, Potts JR (2016) The mathematics behind biological invasions, vol 44. Springer, Cham
Lutscher F (2019) Integrodifference equations in spatial ecology. Springer, Cham
Lutscher F, Nisbet RM, Pachepsky E (2010) Population persistence in the face of advection. Thyroid Res 3(4):271–284
Macfarlane FR, Lorenzi T, Chaplain MAJ (2018) Modelling the immune response to cancer: an individual-based approach accounting for the difference in movement between inactive and activated T cells. Bull Math Biol 80(6):1539–1562
Maini PK, McElwain DLS, Leavesley D (2004) Traveling wave model to interpret a wound-healing cell migration assay for human peritoneal mesothelial cells. Tissue Eng 10(3–4):475–482
Maini PK, McElwain DLS, Leavesley D (2004) Travelling waves in a wound healing assay. Appl Math Lett 17(5):575–580
Murray JD (2002) Mathematical biology: I. An introduction, Springer, New York
Neufeld Z, von Witt W, Lakatos D, Wang J, Hegedus B, Czirok A (2017) The role of Allee effect in modelling post resection recurrence of glioblastoma. PLoS Comput Biol 13(11):e1005818
Petrovskii S, Shigesada N (2001) Some exact solutions of a generalized Fisher equation related to the problem of biological invasion. Math Biosci 172(2):73–94
Saltz D, Rubenstein DI (1995) Population dynamics of a reintroduced asiatic wild ass (Equus hemionus) herd. Ecol Appl 5(2):327–335
Sewalt L, Harley K, van Heijster P, Balasuriya S (2016) Influences of Allee effects in the spreading of malignant tumours. J Theor Biol 394:77–92
Simpson MJ (2009) Depth-averaging errors in reactive transport modeling. Water Resour Res 45:W02505
Simpson MJ, Landman KA, Hughes BD (2009) Multi-species simple exclusion processes. Physica A 388(4):399–406
Simpson MJ, Landman KA, Hughes BD (2009) Pathlines in exclusion processes. Phys Rev E 79(3):031920

Simpson MJ, Landman KA, Hughes BD (2010) Cell invasion with proliferation mechanisms motivated by time-lapse data. Physica A 389(18):3779–3790
Skellam JG (1951) Random dispersal in theoretical populations. Biometrika 38(1/2):196–218
Soboleva TK, Shorten PR, Pleasants AB, Rae AL (2003) Qualitative theory of the spread of a new gene into a resident population. Ecol Model 163(1–2):33–44
Stephens PA, Sutherland WJ, Freckleton RP (1999) What is the Allee effect? Oikos 87(1):185–190
Taylor CM, Hastings A (2005) Allee effects in biological invasions. Ecol Lett 8(8):895–908
Taylor NP, Kim H, Krause AL, Van Gorder RA (2020) A non-local cross-diffusion model of population dynamics I: emergent spatial and spatiotemporal patterns. Bull Math Biol 82(8):112
Treloar KK, Simpson MJ, McElwain DLS, Baker RE (2014) Are in vitro estimates of cell diffusivity and cell proliferation rate sensitive to assay geometry? J Theor Biol 356:71–84
Vortkamp I, Schreiber SJ, Hastings A, Hilker FM (2020) Multiple attractors and long transients in spatially structured populations with an Allee effect. Bull Math Biol 82(6):82
West J, Hasnain Z, Macklin P, Newton PK (2016) An evolutionary model of tumor cell kinetics and the emergence of molecular heterogeneity driving gompertzian growth. SIAM Rev 58(4):716–736
Zhang S, Chong A, Hughes BD (2019) Persistent exclusion processes: Inertia, drift, mixing, and correlation. Phys Rev E 100:042415